5

THE THREE-PULSE PHOTON ECHO

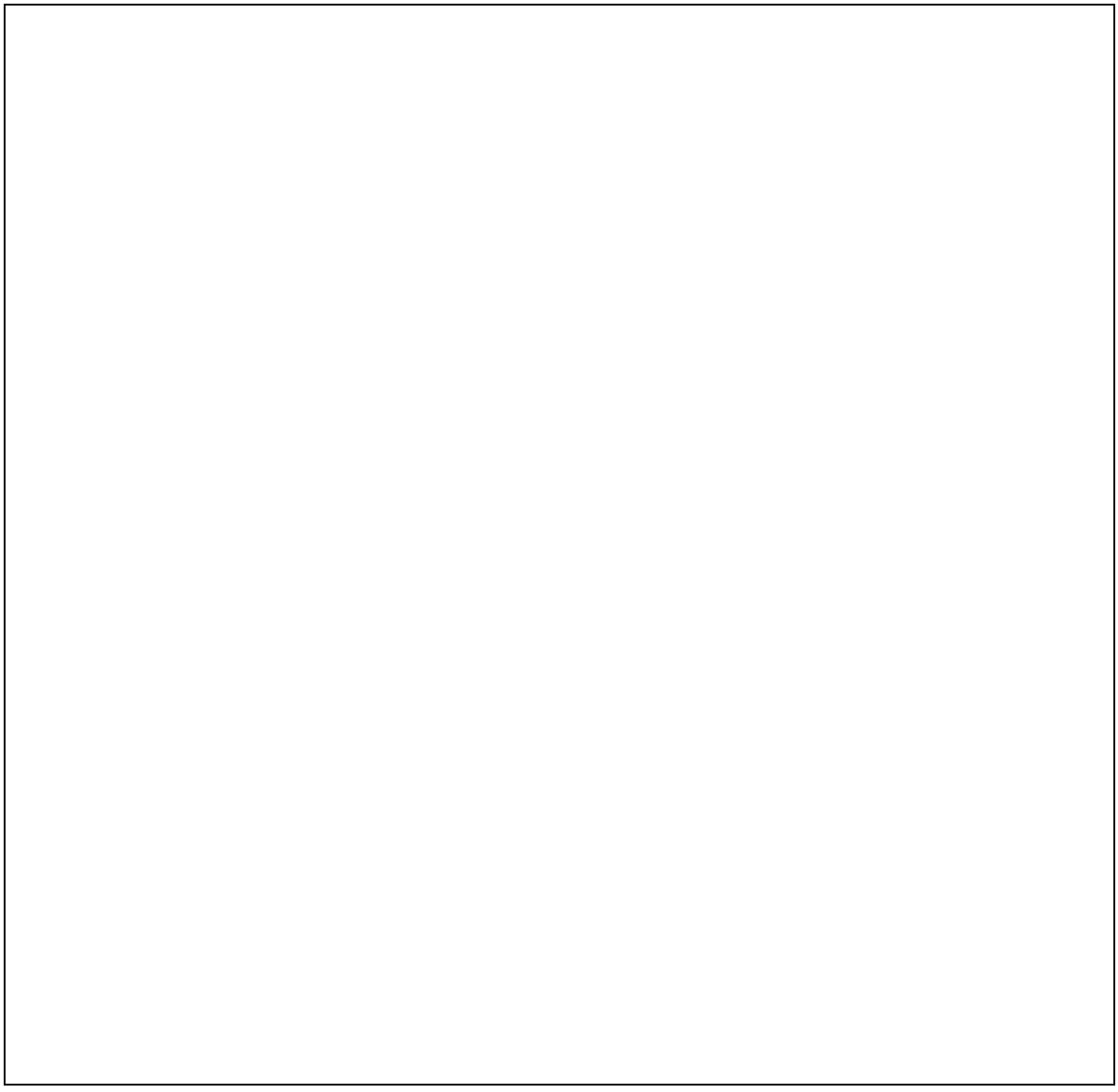

5.1 Introduction

In the previous chapter the dephasing dynamics of the excitons in TDBC aggregates in liquids has been investigated by means of the two-pulse photon echo experiment. In order to obtain more insight in the ultrafast optical dynamics of aggregates and probe the coupling of the aggregates with the surrounding solvent molecules in more detail, the three-pulse stimulated photon echo technique (3PSE) can be employed. By introducing an additional controllable time interval in comparison with the two-pulse photon echo measurement, the time scales of the fluctuations of the aggregate transition frequencies can be characterized over a wide dynamic range. Especially information about the slow fluctuations is obtained, which is interesting in view of the fact that exchange narrowing of the exciton absorption spectrum was shown to be mainly due to a reduction of these slow fluctuations (see chapter 4). Also solvation can be studied in the 3PSE experiment. Solvation, or spectral diffusion, is the frequency analog of spatial diffusion and leads to a shift in energy of the excited states of the aggregates, resulting from solvent relaxation. It can be observed as a time dependent Stokes shift of the fluorescence frequency.

In the three-pulse photon echo experiment, two light pulses excite the sample and form a transient grating. A delayed third pulse scatters from this grating. The type of grating that is formed, depends on the time coincidence of the excitation pulses. The pulse sequence and the two experimentally variable delay times τ and T between the pulses, are depicted in fig. (5.1). When the excitation pulses arrive at the same time, a spatial grating is formed. Increasing the delay time τ between the first two pulses erases the spatial grating, and, instead, gives rise to a frequency grating. The generation of the photon echo can be viewed as the scattering of the third pulse from this frequency grating, analogous to scattering from a spatial grating. The third delayed pulse does not induce a diffracted signal instantaneously, but it triggers rephasing which leads to a stimulated photon echo signal.

The intensity of the stimulated photon echo signal depends on the modulation depth of the grating, implying that processes that reduce the modulation depth lead to a reduction of the echo signal. Variation of delay time τ affects the modulation of the frequency grating by dephasing of coherences. During delay time T between the second and third optical pulse, spectral diffusion tends to erase the grating, and causes the induced frequency grating to blur in time and the magnitude of the gratings to decay to smaller values. In contrast to the two-pulse photon echo experiment, now also population relaxation affects the echo signal by diminishing the magnitude of the gratings. The combined effect of the blurring in frequency and the decaying of excited state population causes the 3PSE signal to decay during delay time T. If the frequency gratings are still present, the third pulse converts them into a coherence, that subsequently will give rise to rephasing and an echo signal is generated. If the delay time T is much larger than the correlation times of the perturbations, the frequency grating has disappeared and a stimulated photon echo is not possible anymore. The 3PSE therefore provides access to the slow component of the correlation function. When τ is not too large, a signal is still possible when the frequency grating has decayed completely, due to the spatial grating that results from the interfering free induction decays induced by the first two pulses. This grating decays by population relaxation only.

The information in the three-pulse echo experiment is two-dimensional: the echo intensity is a function of two delay times, which can be expressed also, if one wishes, as a time and a

frequency axis. Depending on the experimental configuration, one can measure in addition to optical dephasing also solvation dynamics. We will therefore be able to establish a link between solvation and optical dephasing processes. Measuring a τ-dependent decay of the echo signals, with a fixed value of the delay T, provides information on the optical dephasing process induced by the dynamical fluctuations of the liquid surrounding the aggregates. On the other hand, a T-dependent measurement, for a fixed τ, can be used to understand the solvation dynamics and study population relaxation. The solvation dynamics can be probed on longer time scales than that limited by the optical dephasing. Population relaxation will be largely influenced by exciton-exciton annihilation. This aspect will be treated in more detail in chapter 6.

In the analysis of the three-pulse stimulated photon echo experiments, the optical Bloch model does not provide a correct physical basis for the description of optical dephasing of aggregates in solution. In this model no decay of the 3PSE signal is to be expected as a function of T, except for a decay due to population relaxation. The static (inhomogeneous) line broadening is truly static on the time scale of the experiment, so that an echo always will be generated after the third pulse. In order to explain the experimentally observed decay of the stimulated photon echo signal, a more sophisticated theoretical approach is therefore needed.

In the previous chapters we showed that the stochastic model of frequency fluctuations can model data from a number of (non-) linear optical experiments, on different time scales, in a satisfying way. Results of the absorption, the frequency resolved pump-probe, the two-pulse photon echo and the chirped four-wave mixing experiment supported the validity of the stochastic model of frequency fluctuations. It is therefore very likely that the results of the three-pulse stimulated echo experiments, discussed in this chapter, can be interpreted in terms of the same stochastic model. However, solvation, as measured in the 3PSE experiment, cannot be explained in this model. In addition, the stochastic theory fails to account for the Stokes shift of the fluorescence frequency with respect to the absorption. For a phenomenological description of net frequency shifts a more elaborated model for optical dynamics is required and an extension to multiple Brownian oscillators seems then appropriate [1-5].

A particular optical experiment can usually be explained by a variety of models for the optical dynamics, since in each case parameters can be adjusted to yield a best fit to the observed experimental response. It then depends on one's personal taste and the physical relevance of the parameters, which model is preferred for a certain case. Since for aggregates the Stokes shift in emission is small compared to the width of the absorption and emission profiles (see chapter 3, fig. (3.4)), there is no convincing argument for using a more advanced, but also more complicated model. We therefore decided to describe the results of the three-pulse stimulated photon echo experiments within the framework of the stochastic model.

In the experimental section 5.2, results of various stimulated three-pulse echo measurements will be presented. In order to discuss the results of these experiments, the theoretical aspects of the non-linear response functions and three-pulse stimulated echo signals are summarized in sec. 5.3. It is then possible to calculate the response functions associated with the photon echo signals for various fitting parameters. The simulated three-pulse echo signals will be compared with the experimental signals and discussed in sec. 5.4. In the last section 5.5 our findings will be summarized and conclusions will be drawn.

5.2 Three-pulse stimulated photon echo experiments

The lay-out of the three-pulse photon echo experiment of fig. (5.1) has already been shown in chapter 2 (figs. (2.3) and (2.4b)). A short optical pulse with wave vector $\mathbf{k}_1$ creates a coherent superposition of exciton states and the ground state, that subsequently decays due to optical dephasing processes during the first time interval τ. After this evolution period a second short pulse, with wave vector $\mathbf{k}_2$, converts the coherence, with all phase information, into a population grating in the frequency and/or spatial domain, that is, a modulation of population in the optical levels as a function of transition frequency and/or position in the sample. After a second delay time T a third pulse with wave vector $\mathbf{k}_3$ interacts with the grating which will possibly restore the coherence that was lost during delay time τ. Depending on the values of the different delay times, the transient generated during the time t in the direction $\mathbf{k}_2+\mathbf{k}_3-\mathbf{k}_1$ can be characterized either as a photon echo or as an instantaneous diffracted signal.

Two types of measurements are performed. In a first set of measurements, the delay τ is varied, while T is kept constant at a particular value. This type of experiment provides information on the optical dephasing process. A series of stimulated photon echo signals as they were obtained directly from the experiment is shown in fig. (5.2). Only the experimental results for positive values of delay T are presented here. Negative values for delay times T yield the same results, since pulse 2 and 3 are interchangeable due to phase-matching conditions. In this situation $\tau=0$ is then defined as the overlap of pulses 1 and 3, instead of pulses 1 and 2. In a second set of measurements, the delay T is varied, while τ is kept constant. These types of measurements can be used to understand solvation dynamics and obtain information on the correlation times of the frequency fluctuations of the aggregate exciton levels. The results of these experiments are shown in figs. (5.3), for positive and negative values of fixed delay τ. Without going into detail, we will shortly discuss the results of both type of three-pulse photon

echo experiments. They will be treated in more detail in sec. 5.4, by comparing them to calculations.

For the first type of measurements, as a function of delay τ, the experimental results were compared with the case of two-pulse photon echoes. In order to do so it was checked that the three-pulse echo signal observed for delay T=0, was identical to the two-pulse photon echo

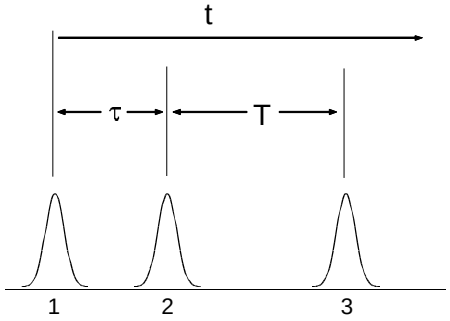

Figure 5.1: The pulse sequence and the two experimentally variable delay times τ and T between the pulses in the three-pulse photon echo experiment.

observed in the direction $2\mathbf{k}_2$-$\mathbf{k}_1$ (as presented in fig. (4.1)). In fig. (5.4) it is shown that both signals agree very well, just as predicted theoretically.

For short delays T, the three-pulse photon echo signals shown in fig. (5.2) are asymmetric. As discussed in the previous chapter, this asymmetry is too strong to be explained by homogeneously broadened transitions. It indicates some degree of inhomogeneity, or more general, non-Markovian behaviour at the time scale of the experiment. With increasing delay T, the measured stimulated photon echo signals in fig (5.2) become more and more symmetrical. This is a signature of a finite, non-Markovian memory time in the optical propagation, causing the echo signal to be transformed into a free induction decay like signal which peaks at zero delay.

The transition from an asymmetric into a symmetric echo signal can adequately be described in terms of Feynman diagrams. In fig. (4.2) it was shown that in a three-level system there are eight independent contributions to the two-pulse photon echo amplitude. For the calculation of the three-pulse stimulated photon echo signal the same Feynman diagrams can be used. The only difference is that what is depicted as pulse 2 in fig. (4.2), can now be either beam 2 or beam 3. We will discuss this in more detail in the next section. At positive delays τ in fig. (5.2), the three-pulse echo signal is mainly formed by rephasing contributions, represented by Feynman diagrams A in fig. (4.2). When there is non-Markovian memory in the propagation of the excitonic system, the amplitude of this signal is higher than for the same negative separation between the pulses, when the signal is formed by the non-rephasing diagrams B and C. When the delay T becomes so long that it exceeds the longest memory time, the difference between the dephasing and rephasing contributions becomes negligible. At this point symmetric echo signals are observed. The delay T at which this transition occurs, will therefore give a clue about the correlation times of the stochastic fluctuations of the aggregate energy levels.

For delay T=0 in fig. (5.2), an echo signal is measured with its maximum at a finite delay τ, close to zero. Any shift from zero delay indicates that rephasing is occurring [6,7], due to the slow

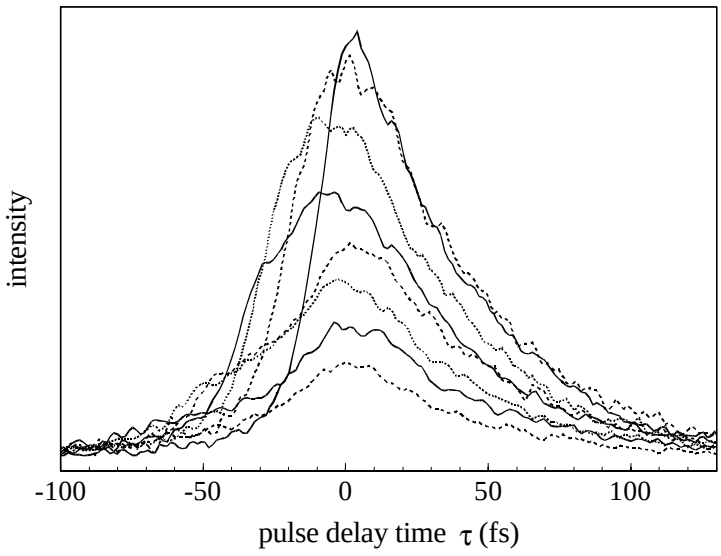

Figure 5.2: Three-pulse photon echo decays of TDBC in water at room temperature in the low pulse energy (perturbative) limit observed in the direction $\mathbf{k}_2+\mathbf{k}_3-\mathbf{k}_1$. The traces are measured as a function of delay time τ for fixed values of the delay time T. Time $\tau=0$ is defined as the time when pulses 1 and 2 overlap in time. Going from the upper curve downwards, the values for T are 0, 10, 20, 30, 40, 50, 60 and 100 fs, respectively.

component of the solvent dynamics. Rephasing in the sample is possible as long as there is memory of the dephasing processes that occurred before. An important factor in the accuracy of the measurements of the shift of the maximum of the three-pulse echo signal, is the determination of zero time. This is performed by a simultaneous measurement of the two mirror image signals in the $\mathbf{k}_2+\mathbf{k}_3-\mathbf{k}_1$ and $\mathbf{k}_1+\mathbf{k}_3-\mathbf{k}_2$ phase matching directions. The exact shift of the echo signals in fig. (5.2) from zero delay is equal to half of the time difference between the two phase-matched signals. However, an extremely high time resolution is required to observe these small shifts [8,9].

For increasing values of T, the maxima of the experimental echo traces of fig. (5.2) seem to shift to negative values of τ and then back to zero. This is somewhat surprising. One would expect that if delay time T becomes larger and starts to exceed the non-Markovian correlation time of the system, optical memory is lost due to spectral diffusion and no rephasing will be possible anymore. The instantaneous grating scattering type signals are then expected to peak at zero delay τ. This occurs in fig. (5.2) for values of T beyond 50 fs. In sec. 5.4, where experimental and theoretical three-pulse echo signals are compared, we will discuss and provide an explanation for the shifting of the maxima of the traces to negative values of τ, when the delay

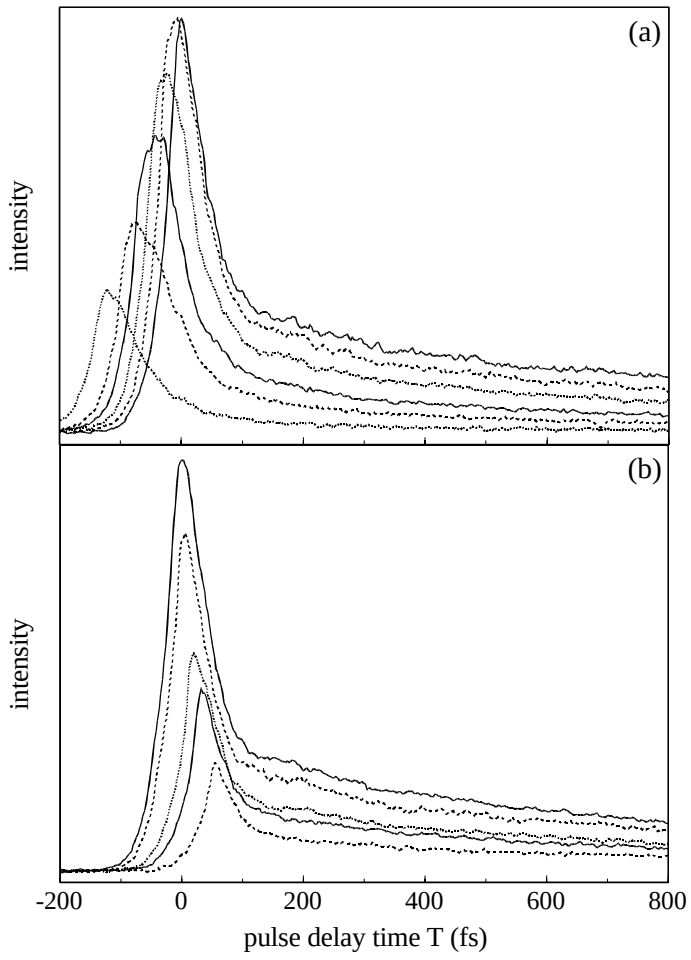

Figure 5.3: A series of stimulated photon echo signals observed in the direction $\mathbf{k}_2+\mathbf{k}_3-\mathbf{k}_1$. Delay time T is varied by scanning pulse 3, while τ is kept constant. At T=0 pulses 3 and 2 overlap in time. (a) The values for τ are, from top to bottom, 0, 20, 40, 60, 80 and 120 fs, respectively. (b) The values for τ are negative and are, from top to bottom, 0, -10, -20, -40 and -60 fs, respectively.

time T is smaller than 50 fs.

The results of the second type of measurements, performed as a function of delay T for a fixed delay τ, are shown in figs. (5.3). They show a maximum in the signal around delay $T=-\tau$, when the scanned third pulse overlaps in time with pulse 1. The strong peak is related to the coherent artefact of the pump-probe experiment discussed in chapter 3. Its origin is not completely clear, but it is observed experimentally that its ultrafast decay resembles the two-pulse echo or the three-pulse echo along the delay time τ for small T. When the third pulse is well separated in time from the excitation beams, a fast decay of the scattering signals to a new equilibrium is observed. The decaying behaviour on longer timescales is not due to solvation dynamics, but to the population lifetime of the aggregates. In chapter 6 we will show that this lifetime is determined by exciton-exciton annihilation processes. The results in figs. (5.3) show that the stimulated echo signals decay faster for larger values of τ. With longer times τ, the modulation period of the frequency population gratings decreases. The gratings then wash out faster with an increasing delay time T, because the solvent perturbations more easily affect a fine grating in frequency space than a rough one, resulting in a faster decrease of the resulting 3PSE signal.

In fig. (5.3a), the trace for delay $\tau=0$ fs represents a real grating scattering signal. The scanned third pulse is scattered from the spatial grating formed by excitation pulses 1 and 2. At zero delay, pulses 1 and 3 also form a grating, that scatters pulse 2 in the direction of observation. When the delay τ between pulses 1 and 2 is increased, with $\tau>0$, these two types of spatial grating scattering can in principle still occur, but also another type of signal is formed. The spatial grating formed by pulses 1 and 2 will decrease with increasing values of τ and instead a frequency grating will arise [10,11]. When the delayed third pulse overlaps with pulse 2, rephasing will be set in action and as long as there is memory, a stimulated photon echo signal will be generated. A rephasing echo signal also arises if pulse 2 and 3 interchange places. The echo and spatial grating scattering signals cannot be distinguished separately, but will shade off into each other.

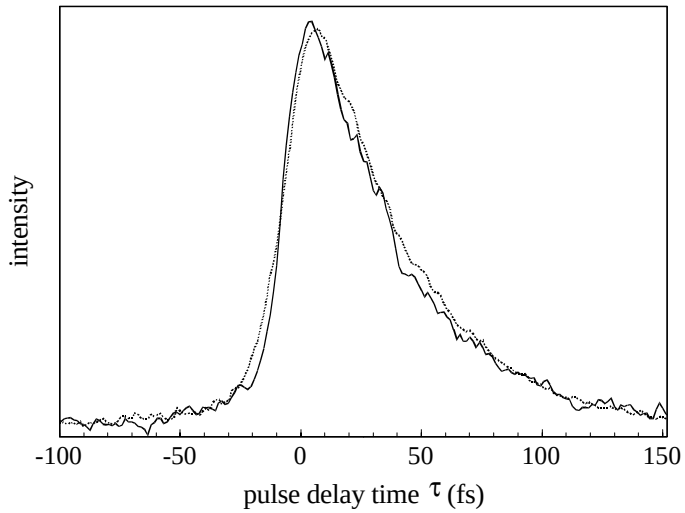

Figure 5.4: Comparison of an experimental three-pulse photon echo signal observed in the direction $\mathbf{k}_2+\mathbf{k}_3-\mathbf{k}_1$, as a function of delay time τ for T=0 fs (solid line), with a two-pulse echo signal observed in the direction $2\mathbf{k}_2-\mathbf{k}_1$ (dotted line).

With a further increase of τ, for values equal and larger than 80 fs, no stimulated echo signals exist anymore. Pulses 1 and 2 are scanned so far apart now, that during time T all phase memory is lost by spectral diffusion and rephasing is not possible anymore. For these large values of τ only an instantaneous spatial grating scattering signal is possible, peaking at delay $T=-\tau$, by the scattering of pulse 2 from the grating formed by pulses 1 and 3.

In fig. (5.3b), the pulse sequence of pulses 1 and 2 is reversed compared to fig. (5.3a), and therefore pulse 2 now always comes first in time. When pulse 3 is scanned and overlaps in time with pulse 2, they form a spatial grating, from which the delayed pulse 1 can scatter. However, this scattered signal will be emitted in the phase-matched directions $\mathbf{k}_1 \pm (\mathbf{k}_2 - \mathbf{k}_3)$ and since the detector is placed in the direction $\mathbf{k}_2 + \mathbf{k}_3 - \mathbf{k}_1$, the signal will not be observed. The grating scattering signal in the phase-matched direction $\mathbf{k}_2 + \mathbf{k}_3 - \mathbf{k}_1$ is only observed if pulse 3 is scanned further and overlaps in time with pulse 1. Basically, the signal is due to the scattering of pulse 3 on the grating formed by the overlapping tails of the free induction decays of the pulses 2 and 1. Therefore the intensity of the signals decreases rapidly with increasing delay between pulses 2 and 1. The signal is never a rephasing echo and peaks always around $T=-\tau$, when pulse 3 overlaps in time with pulse 1.

Before we treat the measured 3PSE signal in more detail by comparing them to some calculations of 3PSE signals in the stochastic model, we will first discuss the theoretical aspects of the echo signals in the next section.

5.3 Theory of the three-pulse stimulated photon echo experiment

The third-order polarization at time t depends on the three optical fields that are applied at earlier times. The non-linear polarization has different contributions, depending on the sequence of the applied fields E_1, E_2 and E_3, and can be written down in the same way as was done for the two-pulse photon echo (eq. (4.11)):

$$\begin{aligned} P^{(3)}(t,T,\tau) \sim \int_0^\infty dt_3 \int_0^\infty dt_2 \int_0^\infty dt_1 \; [& R_3^A(t_3,t_2,t_1)\; E_3(t-\tau-T-t_3) E_2(t-\tau-t_3-t_2) E_1(t-t_3-t_2-t_1) \; + \\ & R_3^B(t_3,t_2,t_1)\; E_3(t-T-\tau-t_3) E_1(t-t_3-t_2) E_2(t-\tau-t_3-t_2-t_1) \; + \\ & R_3^C(t_3,t_2,t_1)\; E_1(t-t_3) E_3(t-T-\tau-t_3-t_2) E_2(t-\tau-t_3-t_2-t_1) \;] \end{aligned} \qquad \textbf{(5.1)}$$

with t_n the time difference between the subsequent interactions, τ the time interval between the envelopes of pulses 1 and 2 and T the time interval between the envelopes of pulses 2 and 3. Time t is counted from the moment that the first interaction occurs. Here the electromagnetic fields are taken to be plane waves (eq. (4.12)). The third-order response or relaxation function R_3 contains the complete microscopic information necessary for the calculation of the optical response, and is here separated in R_3^A, R_3^B and R_3^C, depending on the different pulse permutations.

For evaluation of the three-pulse stimulated photon echo experiment, Feynman diagrams are a feasible way to obtain insight in the relevant dynamics. In the previous section it has already been mentioned that for the calculation of the three-pulse stimulated photon echo, the eight Feynman diagrams of fig. (4.2) can be used. These diagrams describe the formation of the two-pulse photon echo amplitude in the direction $\mathbf{2k}_2\text{-}\mathbf{k}_1$ in a three-level system. However, the three-pulse photon echo is observed in the phase-matched direction $\mathbf{k}_2+\mathbf{k}_3\text{-}\mathbf{k}_1$. This means that what is depicted as pulse 2 in fig. (4.2), can now be either beam 2 or beam 3. Beams 2 and 3 can interchange their role in the order of the interactions around zero delay T, when the delay of both beams is varied relative to each other. So each diagram represents two different situations (pulse 2 before 3 and 3 before 2) and the total number of Feynman diagrams necessary to describe the three-pulse photon echo experiment therefore comes to 16. They describe the six possible permutations which exist for the three pulses and the third-order response function R_3 of eq. (5.1) therefore consists in total out of 6 parts. For the sake of convenience, we call the relaxation functions described by the set of diagrams A, or B or C and with pulse 2 interacting with the sample before pulse 3: R_3^A, R_3^B and R_3^C, respectively. When pulse 2 comes after pulse 3, the matching relaxation functions are called R_3^D, R_3^E and R_3^F, respectively. For the two-pulse photon echo, $R_3^A=R_3^D$, $R_3^B=R_3^E$ and $R_3^C=R_3^F$. For the three-pulse echo they differ because of the explicit introduction of the delay time T between the second and third pulse.

The evaluation of the relaxation functions is performed in the same way as described in sec. 4.3. Again it is assumed that the aggregate energy levels fluctuate stochastically on two characteristic time scales, described by correlation function (4.8) and lineshape function g(t) of eq. (4.9). General expressions for the relaxation functions derived in the previous chapter are then also applicable for the three-pulse echo experiment. Differences occur when the pulse permutations are taken into account.

For diagrams A, the relaxation function is given by eqs. (4.15) and (4.21a). From now on we assume delta-function shaped pulses, so that the triple integrations of eq. (5.1) are readily performed. When the pulse sequence is 123 (pulse 1 arrives first followed by pulses 2 and 3), the delay times read:

$$\begin{aligned} t_1 &= \tau \\ t_2 &= T \\ t_3 &= t-T-\tau \end{aligned}$$

The third-order stochastic relaxation function of eq. (4.21a) then becomes:

$$R_{stoch}^{A}(t,T,\tau) = \exp\{-g(t-T-\tau)-g(\tau)+g(T)-g(T+\tau)-g(t-\tau)+g(t)\} \qquad \textbf{(5.2)}$$

By inserting the appropriate values for the time separations of the pulses in eq. (4.15), the expression for the total relaxation function R_3^A becomes:

$$R_3^A(t,T,\tau) \sim \left[e^{-\frac{1}{2}\gamma_e(t+T)}(1+e^{\gamma_e T}) - \left(\frac{\mu_{2e,e}}{\mu_{e,g}}\right)^2 e^{i(\omega_{eg}-\omega_{2ee})(t-T-\tau) - \frac{1}{2}[\gamma_e(t+T)+\gamma_{2e}(t-T-\tau)]} \right] \times R_{stoch}^A(t,T,\tau) \quad \textbf{(5.3)}$$

with $1/\gamma_e$ and $1/\gamma_{2e}$ the lifetimes of the one- and two-exciton states, respectively.
The pulse sequence in diagrams A can also be 132 (situation D), in which case the times are defined as:

$$\begin{aligned} t_1 &= T+\tau \\ t_2 &= -T \\ t_3 &= t-\tau \end{aligned}$$

The stochastic part of the relaxation function then becomes:

$$R_{stoch}^D(t,T,\tau) = \exp\{-g(t-T-\tau) - g(\tau) + g(-T) - g(T+\tau) - g(t-\tau) + g(t)\} \quad \textbf{(5.4)}$$

and the total relaxation function reads:

$$R_3^D(t,T,\tau) \sim \left[e^{-\frac{1}{2}\gamma_e(t-T)}(1+e^{-\gamma_e T}) - \left(\frac{\mu_{2e,e}}{\mu_{e,g}}\right)^2 e^{i(\omega_{eg}-\omega_{2ee})(t-\tau) - \frac{1}{2}[\gamma_e(t-T)+\gamma_{2e}(t-\tau)]} \right] \times R_{stoch}^D(t,T,\tau) \quad \textbf{(5.5)}$$

For diagrams B, the relaxation functions are given by eqs. (4.17) and (4.21b). The pulse sequence can be either 213 (situation B) or 312 (situation E). The delay times for situation B are then defined as:

$$\begin{aligned} t_1 &= -\tau \\ t_2 &= T+\tau \\ t_3 &= t-T-\tau \end{aligned}$$

and, for situation E, as:

$$\begin{aligned} t_1 &= -T-\tau \\ t_2 &= \tau \\ t_3 &= t-\tau \end{aligned}$$

The stochastic relaxation functions of eq. (4.21b) then become:

$$R^{B}_{stoch}(t,T,\tau) \;=\; \exp\{-g(t-T-\tau)-g(-\tau)+g(T)-g(T+\tau)-g(t-\tau)+g(t)\} \qquad \textbf{(5.6)}$$

and

$$R^{E}_{stoch}(t,T,\tau) \;=\; \exp\{-g(t-T-\tau)-g(\tau)+g(-T)-g(-T-\tau)-g(t-\tau)+g(t)\} \qquad \textbf{(5.7)}$$

respectively. By inserting the appropriate values for the time separations of the pulses in eq. (4.17), the expressions for the total relaxation functions R_3^B and R_3^E can be written as:

$$R_3^{B}(t,T,\tau) \;\sim\; \left[e^{-\frac{1}{2}\gamma_e(t+T)}\left(1+e^{\gamma_e(T+\tau)}\right)-\left(\frac{\mu_{2e,e}}{\mu_{e,g}}\right)^2 e^{i(\omega_{eg}-\omega_{2ee})(t-T-\tau)-\frac{1}{2}[\gamma_e(t+T)+\gamma_{2e}(t-T-\tau)]}\right] \qquad \textbf{(5.8)}$$
$$\times\; R^{B}_{stoch}(t,T,\tau)$$

and

$$R_3^{E}(t,T,\tau) \;\sim\; \left[e^{-\frac{1}{2}\gamma_e(t-T)}\left(1+e^{\gamma_e\tau}\right)-\left(\frac{\mu_{2e,e}}{\mu_{e,g}}\right)^2 e^{i(\omega_{eg}-\omega_{2ee})(t-\tau)-\frac{1}{2}[\gamma_e(t-T)+\gamma_{2e}(t-\tau)]}\right] \qquad \textbf{(5.9)}$$
$$\times\; R^{E}_{stoch}(t,T,\tau)$$

For diagrams C, the relaxation functions are given by eqs. (4.19) and (4.21c). The pulse sequence can be either 231 (situation C) or 321 (situation F) and the delay times are then defined for situation C as:

$$t_1 \;=\; T$$
$$t_2 \;=\; -T-\tau$$
$$t_3 \;=\; t$$

and for situation F as:

$$t_1 \;=\; -T$$
$$t_2 \;=\; -\tau$$
$$t_3 \;=\; t$$

respectively. Then the stochastic relaxation functions eq. (4.21c) become:

$$R_{stoch}^{C}(t,T,\tau) = \exp\{-g(t-T-\tau)-g(-\tau)+g(T)-g(-T-\tau)-g(t-\tau)+g(t)\} \quad \textbf{(5.10)}$$

and

$$R_{stoch}^{F}(t,T,\tau) = \exp\{-g(t-T-\tau)-g(-\tau)+g(-T)-g(-T-\tau)-g(t-\tau)+g(t)\} \quad \textbf{(5.11)}$$

respectively. The total relaxation functions can be written down as:

$$R_3^{C}(t,T,\tau) \sim \left(\frac{\mu_{2e,e}}{\mu_{e,g}}\right)^2 \left[e^{i(\omega_{2ee}-\omega_{eg})(\tau+T)-\frac{1}{2}[\gamma_e(t+T)-\gamma_{2e}(T+\tau)]} - e^{i(\omega_{eg}-\omega_{2ee})(t-T-\tau)-\frac{1}{2}[\gamma_e(t+T)+\gamma_{2e}(t-T-\tau)]}\right] \times R_{stoch}^{C}(t,T,\tau) \quad \textbf{(5.12)}$$

and

$$R_3^{F}(t,T,\tau) \sim \left(\frac{\mu_{2e,e}}{\mu_{e,g}}\right)^2 \left[e^{i(\omega_{2ee}-\omega_{eg})\tau-\frac{1}{2}[\gamma_e(t-T)-\gamma_{2e}\tau]} - e^{i(\omega_{eg}-\omega_{2ee})(t-\tau)-\frac{1}{2}[\gamma_e(t-T)+\gamma_{2e}(t-\tau)]}\right] \times R_{stoch}^{F}(t,T,\tau) \quad \textbf{(5.13)}$$

In Feynman diagrams I, III, IV and VI in fig. (4.2) excited population states exist. Up to now we neglected the fact that relaxation of the one-exciton state |e><e|, after the second excitation pulse, leads to population of the ground state |g><g|. The third pulse then interacts with the ground population state, thus generating an extra contribution to the total signal. Since for aggregates population lifetimes can become very short by exciton-exciton annihilation (see chapter 6) and since in the three-pulse stimulated echo experiment the delay of population period T can become very large, relaxation may occur on comparable timescales as optical dephasing. It is then not enough to just include population relaxation as was done above, but repopulation of lower states also has to be taken into account.

For a proper calculation of the third-order polarization, population feeding should be incorporated into the different relaxation functions. The extra contributions, resulting from the interaction of the third pulse with the relaxed ground population state, from Feynman diagrams I, III, IV and VI in fig. (4.2), lead to Feynman diagrams I′ and IV′ depicted in fig. (5.5). When these are added to the contributions discussed so far, they give rise to slightly different third-order response functions for the situations A, D, B and E.

The extended relaxation function R_3^A eq. (4.15) becomes, after taking into account the extra Feynman diagram I′:

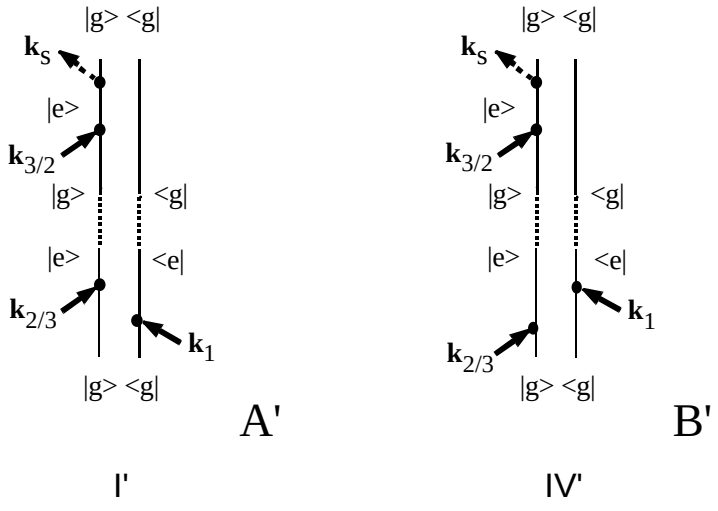

Figure 5.5: Double-sided Feynman diagrams A′ and B′ for three-pulse photon echo generation in a three-level system, consisting of a ground state |g>, a one-exciton state |e>, and a two-exciton state |2e>. The diagrams are additional to diagrams A and B displayed in fig. 4.2 in chapter 4, and take into account that relaxation of state |e><e|, during waiting time t_2, populates state |g><g|. The third pulse then interacts with the ground population, thus generating an extra contribution to the total echo signal. Beams 2 and 3 can interchange their role in the order of the interactions.

$$R_3^{A'}(t_3,t_2,t_1) = [\ 2\mu_{e,g}^4 \left(\exp\{-i\omega_{eg}(t_3 - t_1) - \frac{1}{2}\gamma_e(t_3 + 2t_2 + t_1)\} \right) -$$

$$\mu_{e,g}^2 \mu_{2e,e}^2 \left(\exp\{-i\omega_{2ee} t_3 + i\omega_{eg} t_1 - \frac{1}{2}\gamma_e(t_3 + 2t_2 + t_1) - \frac{1}{2}\gamma_{2e} t_3\} \right)] \qquad \textbf{(5.14)}$$

$$\times \quad R_{stoch}^{A}(t_3,t_2,t_1)$$

By inserting the appropriate values for the time separations of the pulses in eq. (5.14), the expressions for $R_3^{A'}$ and $R_3^{D'}$ can then be rewritten in terms of the time delays t, T and τ as:

$$R_3^{A'}(t,T,\tau) \sim \left[2e^{-\frac{1}{2}\gamma_e(t+T)} - \left(\frac{\mu_{2e,e}}{\mu_{e,g}} \right)^2 e^{i(\omega_{eg} - \omega_{2ee})(t-T-\tau) - \frac{1}{2}[\gamma_e(t+T) + \gamma_{2e}(t-T-\tau)]} \right] \qquad \textbf{(5.15)}$$

$$\times\ R_{stoch}^{A}(t,T,\tau)$$

and

$$R_3^{D'}(t,T,\tau) \sim \left[2e^{-\frac{1}{2}\gamma_e(t-T)} - \left(\frac{\mu_{2e,e}}{\mu_{e,g}} \right)^2 e^{i(\omega_{eg} - \omega_{2ee})(t-\tau) - \frac{1}{2}[\gamma_e(t-T) + \gamma_{2e}(t-\tau)]} \right] \qquad \textbf{(5.16)}$$

$$\times\ R_{stoch}^{D}(t,T,\tau)$$

where the stochastic relaxation functions are given by eqs. (5.2) and (5.4). The above relaxation functions then replace R_3^A and R_3^D given in eqs. (5.3) and (5.5), respectively.

In the same way the time evolution of the total extended relaxation function R_3^B eq. (4.17) can, after taking into account the extra Feynman diagram IV′, be written as:

$$R_3^{B'}(t_3,t_2,t_1) = [2\mu_{e,g}^4 \left(\exp\{-i\omega_{eg}(t_3 + t_1) - \frac{1}{2}\gamma_e(t_3 + 2t_2 + t_1)\} \right) -$$

$$\mu_{e,g}^2 \mu_{2e,e}^2 \left(\exp\{-i\omega_{2ee} t_3 - i\omega_{eg} t_1 - \frac{1}{2}\gamma_e(t_3 + 2t_2 + t_1) - \frac{1}{2}\gamma_{2e} t_3\} \right)] \qquad \textbf{(5.17)}$$

$$\times\ R_{stoch}^{B}(t_3,t_2,t_1)$$

And by inserting the appropriate values for the time separations of the pulses in eq. (5.17), the expressions for $R_3^{B\prime}$ and $R_3^{E\prime}$ can then be rewritten in terms of the time delays t, T and τ as:

$$R_3^{B'}(t,T,\tau) \sim \left[2e^{-\frac{1}{2}\gamma_e(t+T)} - \left(\frac{\mu_{2e,e}}{\mu_{e,g}} \right)^2 e^{i(\omega_{eg}-\omega_{2ee})(t-T-\tau) - \frac{1}{2}[\gamma_e(t+T)+\gamma_{2e}(t-T-\tau)]} \right] \times R_{stoch}^{B}(t,T,\tau) \quad \textbf{(5.18)}$$

and

$$R_3^{E'}(t,T,\tau) \sim \left[2e^{-\frac{1}{2}\gamma_e(t-T)} - \left(\frac{\mu_{2e,e}}{\mu_{e,g}} \right)^2 e^{i(\omega_{eg}-\omega_{2ee})(t-\tau) - \frac{1}{2}[\gamma_e(t-T)+\gamma_{2e}(t-\tau)]} \right] \times R_{stoch}^{E}(t,T,\tau) \quad \textbf{(5.19)}$$

where the stochastic relaxation functions are given by eqs. (5.6) and (5.7). The above relaxation functions then replace R_3^B and R_3^E given in eqs. (5.8) and (5.9), respectively.

The total third-order polarization $P_{3PE}^{(3)}(t,T,\tau)$ for a three-level system is calculated from eq. (5.1). For the calculation of the echo amplitude, we assume a delta-function shape $E_i^0(t)=\delta(t)$ for the amplitude envelop of the optical pulses (eq. (4.12)). The threefold time integrations of the nonlinear polarization in eq. (5.1) are then readily performed, which, as discussed above, gives rise to the expressions eqs. (5.2)-(5.13), (5.15)-(5.16) and (5.18)-(5.19) for the different time orderings of the fields. Hence, for a given t, T and τ, the polarization is determined by only one group of Feynman diagrams and therefore one type of relaxation function:

When pulse 1 is scanned:

If $T\geq 0$	and	$\tau\geq 0$	then	$P_{3PE}^{(3)}(t,T,\tau) \sim R_3^{A'}(t,T,\tau)$ with $t\geq T+\tau$
		$-T<\tau<0$		$P_{3PE}^{(3)}(t,T,\tau) \sim R_3^{B'}(t,T,\tau)$ with $t\geq T+\tau$
		$\tau\leq -T$		$P_{3PE}^{(3)}(t,T,\tau) \sim R_3^{C}(t,T,\tau)$ with $t\geq 0$
If $T<0$	and	$\tau\geq -T$	then	$P_{3PE}^{(3)}(t,T,\tau) \sim R_3^{D'}(t,T,\tau)$ with $t\geq \tau$
		$0<\tau<-T$		$P_{3PE}^{(3)}(t,T,\tau) \sim R_3^{E'}(t,T,\tau)$ with $t\geq \tau$
		$\tau\leq 0$		$P_{3PE}^{(3)}(t,T,\tau) \sim R_3^{F}(t,T,\tau)$ with $t\geq 0$

When pulse 3 is scanned:

If $\tau\geq 0$	and	$T\geq 0$	then	$P_{3PE}^{(3)}(t,T,\tau) \sim R_3^{A'}(t,T,\tau)$ with $t\geq T+\tau$
		$-\tau<T<0$		$P_{3PE}^{(3)}(t,T,\tau) \sim R_3^{D'}(t,T,\tau)$ with $t\geq \tau$

		$T \leq -\tau$		$P_{3PE}^{(3)}(t,T,\tau) \sim R_3^{E'}(t,T,\tau)$ with $t \geq \tau$
If $\tau<0$	and	$T \geq -\tau$	then	$P_{3PE}^{(3)}(t,T,\tau) \sim R_3^{B'}(t,T,\tau)$ with $t \geq T+\tau$
		$0<T<-\tau$		$P_{3PE}^{(3)}(t,T,\tau) \sim R_3^{C}(t,T,\tau)$ with $t \geq 0$
		$T \leq 0$		$P_{3PE}^{(3)}(t,T,\tau) \sim R_3^{F}(t,T,\tau)$ with $t \geq 0$

When pulse 1 is scanned and in the limit of T=0, the expression eq. (4.24) for the two-pulse photon echo results. The echo signals arise at time t, which is counted from the moment that the first pulse enters the sample.

Since the detector integrates the echo intensity over all times t, and the optical pulses have a finite duration, the theoretical expression for the experimentally observed three-pulse stimulated photon echo signal $S_{3PE}(T,\tau)$ is:

$$S_{3PE}(T,\tau) = \left\{ \int_{t_{\min}}^{\infty} [P_{3PE}^{(3)}(t,T,\tau)]^2 dt \right\} \otimes T(T,\tau) \qquad \textbf{(5.20)}$$

where t_{min} depends on the pulse sequence (see above where polarizations are given for different time-orderings of the fields), $\otimes$ designates a convolution and $T(T,\tau)$ is a time resolution function, for which we take the autocorrelation signal.

For finite pulse durations, the non-linear polarizations generated via the different relaxation functions partially overlap in time and consequently interfere. Therefore it is not possible to decompose the total echo signal into several components, like we did above for the non-linear polarizations. Instead all the polarization components should be added up and calculated by explicitly using eq. (5.1), squared and then integrated in time. This process is considerably more time-consuming than the convolution in eq. (5.20) in the delta-pulse limit.

In the next section we will show and discuss the results of the theoretical photon echo curves, calculated in the delta-pulse limit with eq. (5.20), and compare them with the experimental photon echo signals presented in sec. 5.2.

5.4 Model calculations

In this section we present three-pulse stimulated echo signals calculated for a three-level system in the stochastic model, as described in sec. 5.3, and compare them with the experimental results presented in sec. 5.2. In all calculations the dephasing parameters are chosen the same as in the calculations of the two-pulse photon echo signal in chapter 4, with values for the slow fluctuations Δ_{slow}= 10 THz, Λ_{slow}^{-1}= 10 ps and for the fast fluctuations Δ_{fast}= 54 THz, Λ_{fast}^{-1}= 5 fs. Following the interpretation of the pump-probe results, presented in chapter 3, the delocalization length of the aggregates is assumed to be 15 molecules.

The lifetime of the one-exciton band is about 220 ps. Since this lifetime is shortened by exciton-exciton annihilation (see chapter 6), it is more realistic to assume a much shorter lifetime. In the three-pulse photon echo experiment where delay τ is varied for a fixed value of the delay

T, variation of the lifetime in the calculations has no noticeable effect on the shape of the calculated signals, that all decay within 100 fs. The calculations were performed with a lifetime of 10 ps for the one-exciton band. For the other type of three-pulse photon echo experiment, where delay T is varied for a fixed value of τ, the lifetime of the one-exciton band is important. The best simulations of the experimental decays were here obtained with a lifetime of about 4 ps. The difference in lifetimes for different three-pulse photon echo experiments can be explained by a strong dependence on the excitation conditions (see chapter 6).

The lifetime of the two-exciton band must be shorter than any other population relaxation time in the lowest two exciton bands and longer than the timescale of optical dephasing. This specifies the limits for the lifetime of the two-exciton band as 200 fs < $(\gamma_{2e\rightarrow 1e})^{-1}$ < 2 ps (see also chapter 6). In both types of 3PSE experiments, variation of this lifetime has no noticeable effect on the shape of the calculated signals. We assumed a lifetime of 500 fs for the two-exciton band.

5.4.1 The stimulated photon echo as a function of delay τ

In fig. (5.6), calculated three-pulse photon echo signals are presented for the first type of three-pulse photon echo experiment, where delay τ is varied for a fixed value of delay T. Before comparing these results to the experiment (fig. (5.2)), we will first consider several aspects of the calculated echoes in more detail.

In contrast to the experimental results presented in fig. (5.2), the calculated signals in fig. (5.6) show only a slight decrease of intensity as a function of delay T, and only between delay T=0 and 10 fs. With a further increase of time T, the overall amplitude decay of the calculated echo signal is negligible. Because the population decay time of the one-exciton band is in the order of 10 ps, the population decay process can be fully disregarded for the timescales of T in fig. (5.6), ranging up to 100 fs. The slight decrease of intensity between T=0 and 10 fs can be attributed to the loss of the rephasing capability of the contribution of diagrams A of fig. (4.2) (see sec. 5.3). Only for T=0 fs rephasing yields a real echo signal, peaking at a finite delay time τ needed for restoring phase information.

After a fast shift of the position of the maximum to zero delay τ, between T=0 and 10 fs, no change in the positions of the calculated traces in fig. (5.6) can be observed for further increasing values of the delay T. This indicates that rephasing is not very important anymore. So by looking at the positions of the maxima of the calculated signals as a function of delay T, it can be concluded that all phase information is irretrievably lost within 10 fs. This can be compared to the result of the chirped photon echo experiment in chapter 4, where we concluded that after 50 fs, all phase memory has disappeared in the system. From the calculations of the three-pulse photon echo experiment, we can infer now that phase memory is even lost within 10 fs.

We noticed earlier that the asymmetry of the stimulated echo signals in fig. (5.2) may be related to the non-Markovian character of the dynamics of the aggregates. Here we find that even when phase memory is lost for delays T larger than 10 fs, the experimental and theoretical echo signals shown in figs. (5.2) and (5.6) are still asymmetric for delays T up to 50 fs. This can be adequately explained in terms of the different contributions of the Feynman diagrams of fig. (4.2).

At T=0, depicted in fig. (4.2), in the case of positive τ the three-pulse echo signal is formed by the rephasing Feynman diagrams A and by diagrams C for negative delay τ. Increasing the delay T, by introducing a separation of pulses 2 and 3, causes also diagrams B to contribute to the stimulated echo signal, when the pulse sequence is 213 (or 312). We already mentioned in sec. 5.2 that if rephasing is not possible anymore, diagrams A generate a signal for positive delays τ that is identical in intensity with the signal generated by diagrams B for the same, but negative delays $-\tau$. If diagrams A and B equally contribute, a signal will be observed that is symmetric with respect to τ=0. Although phase information is lost for delays T larger than 10 fs, the traces in fig. (5.6) calculated for delays T between 10 and 50 fs, are observed not to be symmetrical. This is due to the fact that diagrams B only contribute to the signal when $-\tau < T$. The contribution of diagrams C for the largest part of the trace, i.e., for $-\tau \geq T$, will induce asymmetrical signals. Only when delay T is large enough, diagrams A and B equally contribute to the signal and the contribution of diagrams C will disappear, resulting in symmetric traces.

Now let us compare the calculated three-pulse photon echo signals in fig. (5.6) with the experimental ones in fig. (5.2). It can be seen that the signal shapes show a significant similarity. The fact that the three-pulse photon echo experiment can be explained in the same stochastic model and with the same dephasing parameters as used for the description of the two-pulse photon echo, the absorption and the pump-probe experiments discussed in the previous chapters, confirms the use of the stochastic model to describe the dynamics of excitons in TDBC aggregates. Also, the changes in the calculated signals in fig. (5.6) with varying values of the delay T, are shown to agree with the experimental ones in fig. (5.2). With increasing delay T, the calculated asymmetric stimulated photon echo signals get more symmetrical, due to an increasing amplitude of the signal for negative delays τ.

When the calculated and the experimental echo signals are compared in more detail, differences can be observed in the positions of their maxima. The maxima of the experimental

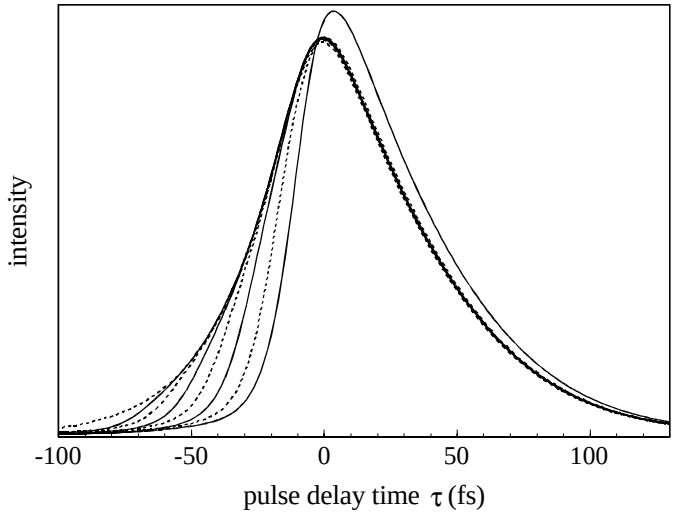

Figure 5.6: A series of theoretical stimulated photon echo signals, calculated in a three-level system within the stochastic model. The signals are based upon eq. (5.20), in which stochastic fluctuations were assumed with correlation times of 5 fs and 10 ps, and amplitudes of 54 and 10 THz, respectively. The exciton delocalization length is 15 molecules. The traces are presented as a function of delay time τ for fixed values of the delay time T. Looking at the rising edge of the curves and going from the right to the left, the values for T are 0, 10, 20, 30, 40, 50, 60, and 100 fs, respectively.

echo traces in fig. (5.2) seem to shift first to negative values of τ and then back to zero delay τ, with increasing values of delay T. The calculated spectra of fig. (5.6) show something different. After a fast shift of the maximum to zero delay τ, between T=0 and 10 fs, no changes in the positions occur anymore for further increasing values of delay T.

In order to facilitate comparison between experiment and theory, the calculated traces of fig. (5.6) were, except the one for T=0 fs, rescaled to the experimental ones of fig. (5.2). The result, for delays T=0, 20, 50 and 100, is shown in fig. (5.7). Now it becomes clear that in the experimental three-pulse echo signals extra contributions are observed in comparison to the calculated traces, at positions where excitation pulses overlap in time. For the T=0 trace in fig. (5.7) an extra contribution can be seen clearly around τ=0, when pulse 1 overlaps in time with pulses 2 and 3. For traces with larger values of the delay T, this extra intensity of the experimental signals, compared to the calculated ones, has disappeared because traces were rescaled. When pulse 1 overlaps in time with pulse 3, a bump is observed in all experimental signals, compared to the calculated ones. These bumps occur for the different traces in fig. (5.7) at values of $-\tau$=T. They induce the artificial shifts of the maxima of the echo signals.

The biggest discrepancy between the calculated and experimental results is the rapid decay of the experimental signal when T is increased. This shows up even more clearly when the echo is measured directly along that time variable. This will be discussed further in sec. 5.4.2 (see in particular figs. (5.3) and (5.9)). All traces show a distinct peak around T=0, which is not observed in the calculated signals. This extra contribution made rescaling of the calculated signals necessary.

Apparently, the situations in which excitation pulses overlap in time are not described correctly in the employed model. One approximation we made which can possibly explain the difference between theory and experiment, is that we assumed delta-function shaped optical excitation pulses in the calculations. In order to check this statement, some stimulated echo

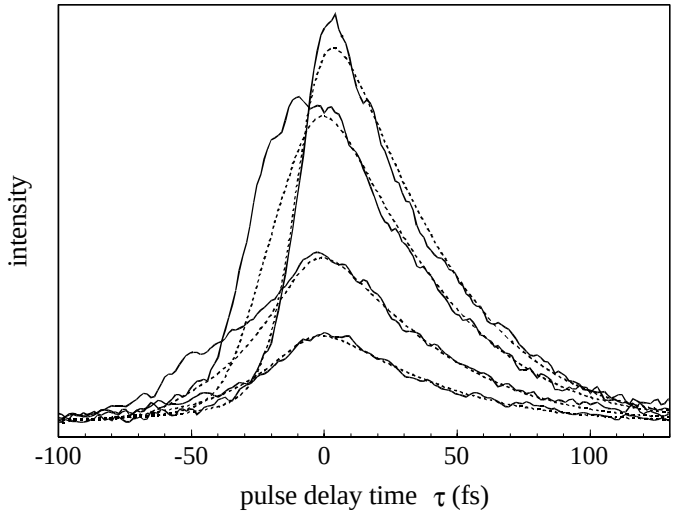

Figure 5.7: Comparison between experimental and theoretical stimulated photon echo signals of TDBC in water, as a function of delay time τ. The traces are, going from the upper curve downwards, given for fixed values of the delay time T of 0, 20, 50 and 100 fs, resp. The solid lines are experimental three-pulse photon echo decays, reproduced from fig. 5.1. The dashed curves represent calculated three-pulse photon echo signals in the stochastic model and are reproduced from fig. 5.5. In order to facilitate comparison between experiment and theory, the calculated traces were rescaled to the experimental ones, except the one for T=0 fs.

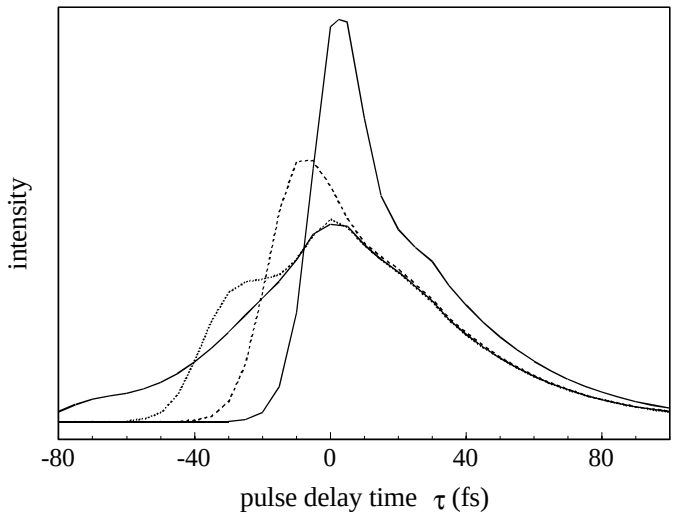

Figure 5.8: Theoretical stimulated photon echo signals, calculated in a two-level system for pulses with a finite pulse duration of 10 fs. Quasi-resonant excitation is assumed ($\Delta\omega$=0.17 fs^{-1}). The traces are presented as a function of delay time τ for fixed values of the delay time T of, going from the upper curve downwards, 0 (solid), 20 (dashed), 40 (dotted) and 80 fs (solid), respectively.

signals were calculated for pulses with finite pulse durations.

For this aim, threefold time integrations need to be performed for calculation of the nonlinear polarization eq. (5.1), which are very time-consuming. In order to simplify the calculations, the third-order polarization was calculated in a two-level system. In that case only Feynman diagrams I and II of terms A and diagrams IV and V of terms B in fig. (4.2) contribute. The optical pulses eq. (4.12) are assumed to have a width of 10 fs, with an amplitude envelop $E_i^0(t)$, described by a quadratic hyperbolic secant ($\mathrm{sech}^2(t)$) [5]. The theoretical expression for the stimulated photon echo signal is then not described by a convolution such as eq. (5.20), but by an integral over the nonlinear polarization:

$$S_{3PE}(T,\tau) = \int_t^\infty [P_{3PE}^{(3)}(t,T,\tau)]^2\, dt \qquad \textbf{(5.21)}$$

Since the central wavelength of the excitation pulses is 620 nm and the absorption wavelength of the TDBC aggregates is 587 nm, a quasi-resonant excitation can now be taken into account, which is impossible when delta-function shaped pulses are assumed. The results of the echo calculations are shown in fig. (5.8) for four different values of the delay T.

When the echo traces in fig. (5.8) are compared with the calculated ones presented in fig. (5.6), it is clear that by taking into account a finite width of the optical pulses, distinctly different stimulated echo signals are obtained. For the signals presented in fig. (5.8), the intensities now have a much stronger dependence on the delay time T, meaning that extra contributions are generated when pulses 2 and 3 overlap in time. Extra contributions are also clearly observed at values of the delay $-\tau$=T, i.e., at points were pulse 1 overlaps in time with pulse 3. This all agrees very well with what we observed experimentally. These findings are strongly dependent on the

excitation condition. If resonant excitation is assumed, smooth stimulated echo curves were obtained, of the type shown in fig. (5.6).

The assumption of the finite pulse duration compared to the previous calculation therefore has two effects. First, while the pulses overlap, more than one permutation of the fields contribute to the signals. Second, the detuning of the central frequency of the excitation pulses from the excitonic resonances causes extra bumps in the signal traces along both time axes. This is the reason why in fig. (5.8), in the echo trace calculated for T=0, a small shoulder is visible around τ=25 fs. It is not observed experimentally, probably because of the low intensity. Since both of these effects reflect details in the optical interactions, rather than provide information on the exciton dynamics, we will not discuss them any further here.

5.4.2 The stimulated photon echo as a function of delay T

In figs. (5.9), calculations are presented for the other type of three-pulse stimulated echo experiment: now the delay T is varied, for a fixed delay τ. A distinction can be made between the echo signals calculated for values of the delay $\tau \geq 0$, as presented in fig. (5.9a), and those measured for values of $\tau \leq 0$, shown in fig. (5.9b). They simulate the experimental stimulated photon echo results presented in figs. (5.3a) and (5.3b), respectively. Before comparing the calculated results with the experimental ones, we will first discuss them shortly.

The calculated results in fig. (5.9a), where $\tau \geq 0$, show in fact two types of decay. For τ=0 a slow decay is visible of the spatial grating formed by the temporally overlapping pulses 1 and 2, from which pulse 3 scatters. This decay is due to population decay of the aggregates, speeded up by exciton-exciton annihilation. This will be discussed more extensively in chapter 6. For the largest value of τ a very fast decay can be noticed, caused by the scattering of pulse 2 on the grating formed by pulses 1 and 3. Because pulse 3 is delayed in time with respect to pulse 1, the grating is disappearing quickly and the signal intensity decreases rapidly. In fig. (5.9b) only the first type of grating scattering is possible, since pulse 2 reaches the sample before the spatial grating of pulses 1 and 3 is formed.

In both figs. (5.9) the positions of the maxima are always centred around $T=-\tau$, i.e., when pulse 3 overlaps in time with pulse 1. This is somewhat surprising for the curves calculated for $\tau>0$, since there one would expect to observe some rephasing echo effects. Also the shapes of the calculated traces do not clearly reveal any echo character, only grating scattering type signals are easily recognizable. The grating scattering peak around delay $T=-\tau$ can be seen to appear already for delay $\tau=20$ fs. For larger delays τ it becomes perfectly symmetric. If significant rephasing would occur, one would expect the rephasing photon echo signals to dominate the ingrowth of the spatial grating scattering peak. For larger delays τ the spatial grating should always become stronger than the echo, since then the phase memory of the system is lost and rephasing is not possible anymore. For the dynamical parameters assumed here, apparently all phase memory in the system is rapidly lost. This supports our conclusion from the previous section, where we discussed the other type of three-pulse photon echo experiment.

When the calculated three-pulse photon echo signals are compared with the experimental

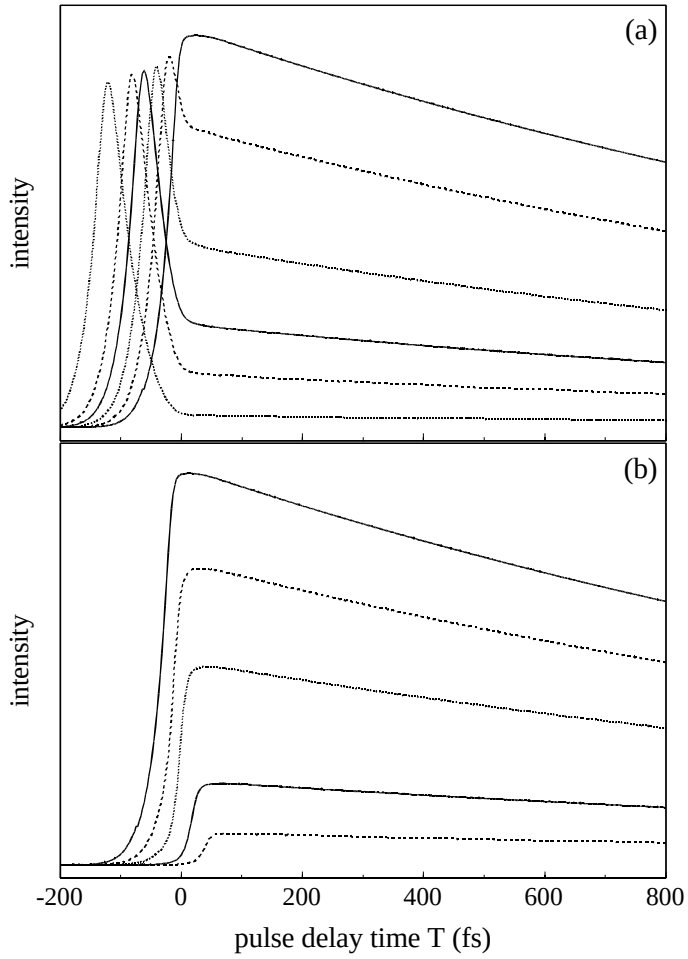

Figure 5.9: A series of theoretical stimulated photon echo signals, calculated in a three-level system in the stochastic model. The signals are based upon eq. (5.20), in which stochastic fluctuations were assumed with correlation times of 5 fs and 10 ps, and amplitudes of 54 and 10 THz, respectively. The exciton delocalization length is 15 molecules. The traces are presented as a function of delay time T for fixed values of the delay time τ. (a) The values for τ are, from top to bottom and from right to left, 0, 20, 40, 60, 80 and 120 fs, respectively. (b) The values for τ are negative and are, from top to bottom, 0, -10, -20, -40 and -60 fs, respectively.

ones in figs. (5.3), the fits are seen to be far from satisfactory. It seems impossible to simulate the experimental behaviour around delay $T=-\tau$. The sharp peak, observed when pulses 3 and 1 are overlapping in time, is also observed by Mittleman et al. [12], while probing the dynamics of quantum-confined excitons in nanocrystals of CdSe with three-pulse photon echo experiments. There the peak becomes more prominent with decreasing size of the nanocrystals, i.e., with increasing confinement of the excitons. It is possible that the peak is one of those extra contributions arising with overlapping excitation pulses, which were discussed in sec. 5.4.1. It seems that also here the finite pulse duration and the off-resonance excitation frequency are, to some extent, responsible for the observed discrepancies. However, it is also possible that by these three-pulse echo experiments some limitations of the dynamical model are revealed.

The experimental traces and the calculations performed in the stochastic model are compared in more detail in fig. (5.10) for two different delays, $\tau=0$ and $\tau=120$ fs. For delay $\tau=0$ the huge difference between experiment and theory is clearly visible. The peak around zero delay cannot be calculated in the stochastic model as we used it. Only the tail of the experimental decay, for large values of T, can be fitted. For delay $\tau=120$ fs the calculated trace is rescaled on the experimental one, in order to make comparison possible by compensating for the extra contribution in intensity which is observed when pulses 1 and 3 are overlapping in time. Still, experiment and theory do not agree. The experimental peak around $T=-120$ fs is asymmetric and much broader than the theoretical prediction. One explanation could be that by an instability in the experimental set-up the experiment is performed with pulses much broader than 10 fs. However, we were able to reproduce this signal in other experimental series, performed on different days. It is more likely that the experimental peak is broadened by an extra contribution to the signal around T=0 fs, when excitation pulses 2 and 3 are overlapping in time. This extra contribution is probably also the reason for the artificial shift of the maxima of the experimental signals for delays $\tau=20$, 40 and 60 fs in fig. (5.3a). These traces seem to shift from their $T=-\tau$

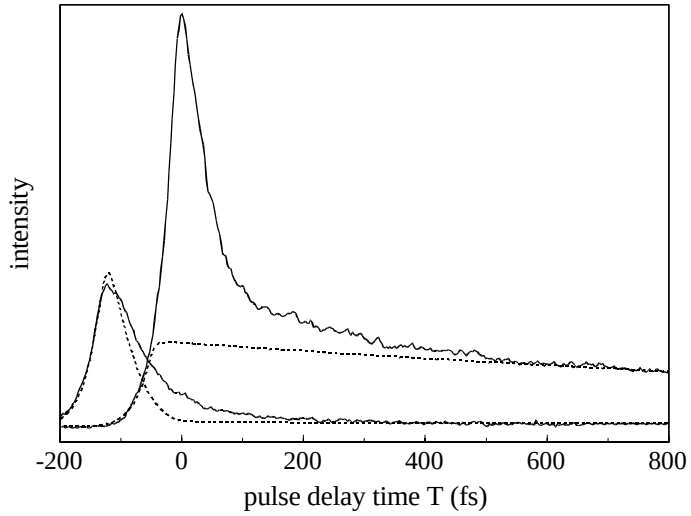

Figure 5.10: Comparison between experimental and theoretical stimulated photon echo signals of TDBC in water, as a function of delay time T. The solid lines are experimental three-pulse photon echo decays, reproduced from fig. (5.3a), for fixed values of the delay time τ of 0 (upper curve) and 120 fs (lower curve). The dashed curves represent the corresponding calculated three-pulse photon echo signals in the stochastic model and are reproduced from fig. (5.9a). In order to facilitate comparison between experiment and theory, the calculated trace for $\tau=120$ fs was rescaled to the experimental one.

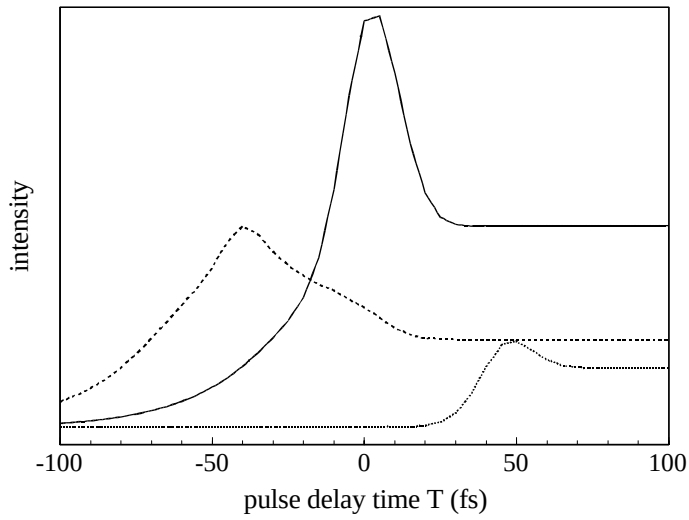

Figure 5.11: Theoretical stimulated photon echo signals, calculated in a two-level system for pulses with a finite pulse duration of 10 fs. Quasi-resonant excitation is assumed, similar as in the calculation of fig. (5.8). The traces are presented as a function of delay time T for fixed values of the delay time τ of 0 (solid), 40 (dashed) and –40 fs (dotted).

position, as predicted in the calculations of fig. (5.9a), towards zero delay T, although this may be a bit difficult to observe in the presented figure.

In order to check the effect of the use of optical pulses with a finite pulse duration on the shape of the three-pulse stimulated echo signals, some signals were calculated for pulses with finite pulse durations, instead of delta-function shaped pulses, in a way as described in sec. 5.4.1 (eq. (5.21)). Again the excitations are assumed to be quasi-resonant. The results of the calculations are presented in fig. (5.11) for three different values of the delay τ. When they are compared with the calculated traces of figs. (5.9), one can notice that now a peak is appearing around delay $T=-\tau$, although not as pronounced as observed experimentally. The peak is not seen when a resonant excitation is assumed. The decay of the calculated curves for longer values of T is much slower, or is even lacking, compared to the experimental traces, but this can be explained by the fact that in order to facilitate the calculations, population decay was ignored.

5.5 Summary and conclusions

In this chapter results on the three-pulse stimulated photon echo technique have been presented. The results were analysed in a stochastic model of frequency fluctuations. In previous chapters, this model was already successfully used in the analysis of the two-pulse photon echo, the chirped photon echo, the absorption, and the pump-probe experiment. The model seems to be somewhat less successful to explain the observed results of the three-pulse photon echo experiment with the same dephasing parameters.

Problems arise in particular when the excitation pulses overlap in time. By taking into account a finite width of the optical excitation pulses, instead of delta-function shaped pulses, and assuming the excitations to be quasi-resonant, the agreement between the calculations and the

experiments improves considerably. However, this can not completely explain the strong peak that is observed in the T-dependent scans when pulses 1 and 3 overlap in time. It may reflect exciton dynamics that is not taken into account in our stochastic model. For instance, the exciton may slightly localize after the optical excitation, thereby altering the transition moment, in analogy to the dynamic non-Condon effect. Some credibility to this type of model was recently obtained, when it was established that the decay of the strong peak at $T=-\tau$ is identical to that of the two-pulse photon echo [13]. However, the validity of this explanation remains an open question as long as no definite experimental proof has been given.

The limitations revealed by the three-pulse photon echo experiments may also be partly due to the fact that solvation is not taken into account in the stochastic model. This model is in principle only valid in the high temperature limit, in which the transition frequency of the propagating system is much smaller than kT. In this situation only fluctuations of the transition frequency occur. There is no net energy transfer between the system and the surrounding heat bath that induces the fluctuations of the system. However, for optical excitations at room temperature, this high temperature limit does not hold. Therefore, energy will usually be transferred between the system and the heat bath when the state of the system is changed. Due to solvation, the rearrangements of the solvent molecules directly around the excited system, a time dependent shift of the transition frequency occurs, which can be observed as a Stokes shift. For a phenomenological description of these effects a more general approach to optical dynamics is required than provided by the stochastic model [3-5,8]. However, in our case the relatively small Stokes shift of aggregates (see chapter 3, fig. (3.4)) provides support for the stochastic treatment as presented in this chapter.

The three-pulse stimulated echo experiments reveal that the phase memory disappears extremely fast in this system, possibly within 10 fs. The slow fluctuations, with a correlation time of 10 ps, are clearly less important. This finding is expected for photon echoes, and agrees well with the conclusion of Cho and Fleming that such measurements preferentially detect the fastest solvent fluctuations [14].

The stochastic model is a phenomenological model, veiling the microscopic details on the mechanisms of the dynamic behaviour of aggregates. For this reason, the challenge of revealing the physical basis of the dynamics of aggregates in solutions still exists. The development of a more microscopic model requires additional experimental information. Recently, Cho and Fleming proposed a new spectroscopic technique which provides additional information on the dynamics of molecules or aggregates: the fifth-order three-pulse photon echo (F3PE) experiment [14]. Previously this technique was known as the image echo [10]. Especially the inertial nature of the early (<100 fs) solvation dynamics can be revealed with this type of experiment [8,14]. The optical polarization excited by two pulses is interrogated in the sample by a third pulse. It can be considered as a form of time-gated two-pulse photon echo spectroscopy, but its theoretical description and numerical calculation are more complicated. Some preliminary F3PE experiments were performed on TDBC aggregates [13]. In addition, from another form of the three-pulse stimulated photon echo, referred to as three-pulse stimulated photon echo peak shift measurements, the contribution of the very slow or static (inhomogeneous) component to the dynamics can be obtained [9,15-17]. A very stable experimental set-up is then required. This type of experiment was also recently performed on TDBC aggregates [13]. The outcome of both

experiments can perhaps shine more light on the detailed nature of the dynamics of aggregates in solution.

References

1. Y.J. Yan and S. Mukamel, J. Phys. Chem. **89**, 5160 (1988).
2. Y.J. Yan and S. Mukamel, Phys. Rev. **A41**, 6485 (1990).
3. E.T.J. Nibbering, D.A. Wiersma and K. Duppen, Chem. Phys. **183**, 167 (1994).
4. S. Mukamel, *Principles of Nonlinear Optical Spectroscopy*, Oxford, New York, 1995.
5. W.P. de Boeij, M.S. Pshenichnikov and D.A. Wiersma, J. Phys. Chem. **100**, 11806 (1996).
6. T. Joo and A.C. Albrecht, Chem. Phys. **176**, 233 (1993).
7. A.M. Weiner, S. De Silvestri and E.P. Ippen, J. Opt. Soc. Am. B **2**, 654 (1985).
8. T. Joo, Y. Jia and G.R. Fleming, J. Chem. Phys. **102**, 4063 (1995).
9. W.P. de Boeij, M.S. Pshenichnikov and D.A. Wiersma, Chem. Phys. Lett. **253**, 53 (1996).
10. K. Duppen and D.A. Wiersma, J. Opt. Soc. Am. B **3**, 614 (1986).
11. D.A. Wiersma and K. Duppen, Science **237**, 1147 (1987).
12. D.M. Mittleman, R.W. Schoenlein, J.J. Shiang, V.L. Colvin, A.P. Alivisatos and C.V. Shank, Phys. Rev. **B49**, 14435 (1994).
13. A.M. Renier, unpublished results.
14. M. Cho and G.R. Fleming, J. Phys. Chem. **98**, 3478 (1994).
15. T. Joo, Y. Jia, J.-Y. Yu, M. J. Lang and G.R. Fleming, J. Chem. Phys. **104**, 6089 (1996).
16. S.A. Passino, Y. Nagasawa, T. Joo and G.R. Fleming, J. Phys. Chem. A **101**, 725 (1997).
17. T. Joo, Y. Jia, J.-Y. Yu, D.M. Jonas and G.R. Fleming, J. Phys. Chem. **100**, 2399 (1996).